# Modeling of breakdown behavior in radio-frequency argon discharges with improved secondary emission model

M. Radmilović-Radjenović and J. K. Lee
*Electronics and Electrical Engineering Department, Pohang University of Science and Technology, Pohang 790-784, Republic of Korea*

(Received 31 January 2005; accepted 6 April 2005; published online 26 May 2005)

This work represents the investigation of the dependence of the breakdown voltage on the gas pressure and on the frequency in radio-frequency argon discharges. Calculations were performed by using a one-dimensional particle-in-cell/Monte Carlo code with three velocity components with a new secondary emission model. The obtained results show that the multivalued nature of the left-hand branch of the breakdown curve can be achieved only by taking into account energy dependence of the yield per ion. The multivalued nature of the left-hand branch of the breakdown curve is attributed to the influence of the secondary emission characteristics of the electrodes on the breakdown voltage. Simulation results show a good agreement with the available experimental data. Disagreements between simulation results and theoretical predictions based on the phenomenological method indicate that a more accurate determination of molecular constants is needed. As a result of the satisfactory agreement between simulation and experimental data for dependence of the breakdown voltage on the frequency, a frequency scaling law is proposed.
 [DOI: 10.1063/1.1922267]

## I. INTRODUCTION

It is well known that studies of the nonequilibrium processes which occur in radio-frequency (rf) discharges during breakdown are of interest both for industrial applications[1–3] and for a deeper understanding of fundamental plasma behavior.[4–6] Capacitively coupled rf discharges are receiving an increased attention due to their wide applications in many technological processes such as plasma etching for semiconductor materials,[7,8] thin film deposition,[9,10] and plasma cleaning.[11] In order to optimize plasma technological processes, it is often necessary to know gas breakdown conditions in a discharge device. Therefore, it is of considerable interest to simulate and measure the breakdown curves in rf fields.

Argon is important as a benchmark gas in the discharge studies. Numerous experimental and theoretical papers have been published on capacitively coupled rf discharges in argon.[12–14] However, as far as rf argon breakdown is concerned, agreement between the measured and the predicted criteria is unsatisfactory. In trying to improve the agreement between the theory[15] and the measured data,[16] Sen and Ghosh[17] suggested revising the numerical values of the molecular constants used by Kihara.[15] Lisovskiy and his co-worker[18] applied a phenomenological method based on the earlier breakdown theory[15] adjusting the molecular constants in the breakdown formula and using measured breakdown voltages to obtain proper agreement between the observation and the prediction but the results were still unsatisfactory. Sato and Shoji[19] derived the breakdown criteria from the electron balance model in a two-dimensional geometry and achieved a good agreement between theoretical prediction and measured breakdown characteristics in the case of short electrode separations. Smith *et al.*[20] used a one-dimensional particle-in-cell (PIC) simulation to investigate the effect of the secondary emission characteristics of the electrodes on the breakdown voltage and then simulation and experimental results have been used in the development of a zero-dimensional global (volume averaged) model of rf breakdown. In recent years, computer modeling and simulation have emerged as effective tools that complement the laboratory experiments and the analytic models.[20–22]

Typically, Paschen curves are roughly "u" shaped with a minimum breakdown voltage at a specific $pd$ and increasing voltages at both increasing and decreasing values of $pd$.[18–20,23] The breakdown voltage generally forms a fairly smooth curve, with the left-hand branch of the curve being markedly steeper than the right-hand branch. But, under certain circumstances inflection points and other changes in the slope of the breakdown curves have been measured.[24,25] It was found that the left-hand branch of the breakdown curve is a multivalued function of the gas pressure, i.e., a single gas pressure corresponds to several breakdown voltages. The multivalued nature of the left-hand branch of the breakdown curve is seen both at small and at large distances between the electrodes. The right-hand branch of the breakdown curve has an inflection point, but only if the distance between the electrodes is small, and the minimum of the curve lies at a pressure for which the electron-neutral collision rate is much larger than the frequency of the electric field. The deviation of the left-hand branch of the breakdown curve into the high-pressure region can also be observed. As the voltage is increased, the emission from the electrodes increases and the breakdown curve shifts to the low-pressure region.[24,25]

In this paper, particle-in-cell/Monte Carlo simulations have been extensively used to investigate a region of an ambiguous dependence of rf breakdown voltage on the gas pressure to the left of the minimum of the breakdown curves.[24,25] Our simulation results show that such an ambiguity region

 

appears in rf discharges during the breakdown not only by increasing the rf voltage but also by decreasing it. In other words, on lowering the pressure, the rf voltage first decreases and passes through an inflection point and a minimum on the breakdown curve, and then it grows and approaches the turning point on the breakdown curve. In addition, dependence of the breakdown voltage on frequency is also studied. Obtained simulation results are systematically analyzed and a scaling law that corresponds to this dependence has been suggested.

## II. RADIO-FREQUENCY DISCHARGES

### A. Breakdown mechanism

In rf discharges, electrons can attain oscillatory energy from the ac field. When an electron suffers a collision, its oscillatory motion is disturbed and its momentum is randomized. In order to determine the servitude of the breakdown field strength on the gas pressure, we can regard the discharge as a diffusion-controlled one, i.e., a discharge in which diffusion loss is the primary loss mechanism. In the steady state, this loss will be balanced by ionization and described by the relation

$$\frac{\nu_I}{D} = \frac{1}{\lambda_D^2}, \tag{1}$$

where $\nu_I$ is the ionization frequency, $D = T_e/m_e\nu_c$ is the diffusion coefficient, and $\lambda_D$ is the diffusion scale length. In the limit of moderately high pressures where $\nu_c \gg \omega$ ($\nu_c$ is the collision frequency and $\omega$ is the angular frequency of the rf applied field) large number of collisions take place within a wave period, so that the electrons are unable to gain their steady-state oscillation energy and thus large electric field is needed to initiate the breakdown. In the low-pressure limit ($\nu_c \ll \omega$), collisions are few and far between, so that many cycles of the wave period go by before a collision occurs and the field strength again rises. It follows that the breakdown field increases both in the high- and low-pressure regimes. This indicates that between them, there must be a region where the breakdown field has a minimum. This minimum occurs at a pressure for which $\omega \approx \nu_c$.

### B. Discharge as a function of frequency

A beneficial limit that characterizes the rf discharges is the so-called "oscillation amplitude limit" which occurs when the oscillation amplitude $x_0$ of a charged particle, given by the expression (see, for example, Ref. 26)

$$x_{0e,i} = \frac{e_{e,i}E_0}{m_{e,i}\omega(\nu_{ce,i}^2 + \omega^2)^{1/2}} \tag{2}$$

becomes comparable to a relevant chamber dimension $d$, i.e., $x_0 \approx d/2$. In Eq. (1) subscripts $e$ and $i$ are related to electrons and ions, respectively. Dependence of the breakdown field on the rf wavelength near the oscillation amplitude limit is shown in Fig. 1. At very low frequencies, both electrons and ions are able to respond to the ac fields quickly and the oscillation amplitude for both species is well beyond the oscillation limit, i.e., $x_0 \gg d/2$. Both species therefore hit the chamber walls and hence present a major loss for the system. Thus, plasma is sustained by secondary electrons produced by ion bombardment of the cathode.

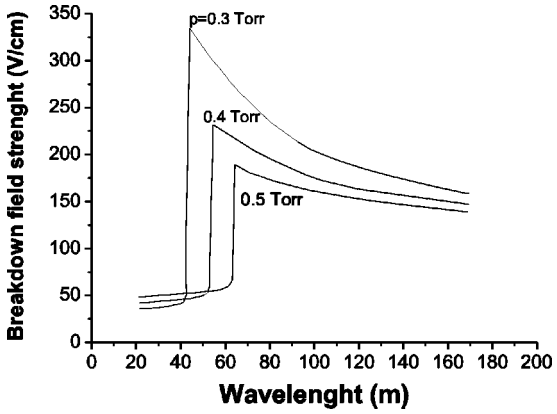


FIG. 1. Dependence of the measured breakdown field strength on the rf wavelength near the oscillation amplitude limit for three different values of the gas pressure (Ref. 26).

As frequency is increased, the ion response to the ac field becomes more deliberate, although the electrons follow the ac fields without any difficulty. Thus, the ion current to the cathode decreases so that the ion bombardment and the secondary electron production are depleted. Such reduced secondary electron production is compensated by an increase in the breakdown field as can be observed clearly in Fig. 1.

Further increase of the frequency causes a sharp reduction in the ion bombardment of the cathode along and consequently in the secondary electron production. This situation occurs typically for rf discharges at frequencies around a few megahertz. At these frequencies, the ions cannot respond to the rf fields, but the electron response is almost instantaneous and the electron loss quite severe. Due to the high deficit of secondary electrons, the discharge is difficult to maintain and the breakdown field strength rises steeply. As the frequency is raised further, the maximum deflection of electrons becomes smaller compared to the oscillation amplitude limit and consequently the loss of electrons and the breakdown field strength drops abruptly.

### C. Phenomenological theory of breakdown

In describing the rf breakdown let us start from the Kihara equation (see, for example, Ref. 15) that gives the condition for the rf gas breakdown:

$$e^{B_0 p/2E} = A_1 pd\left(1 - \frac{E/B_0 p}{C_2 d/\lambda}\right), \tag{3}$$

where $E = E_{\mathrm{rf}}/\sqrt{2}$ is the effective rf field, $p$ is the gas pressure, $d$ is the electrode spacing, $\lambda$ is the vacuum wavelength of the rf field, and finally, $A_1$, $B_0$, and $C_2$ are the molecular constants. In order to dispose the position of the minimum and the turning point on the breakdown curve, we find the first derivate of Eq. (3) and using conditions $dU_{\mathrm{rf}}/dp = 0$ and $dU_{\mathrm{rf}}/dp = \infty$ for the minimum and the turning point, respectively, we obtain the following expressions:

$$p_{\text{minimum}} = \frac{\left(1+\frac{\lambda}{2C_2d}\right)}{A_1 d}\exp\left(1+\frac{\lambda}{2C_2d}\right),$$

$$(U_{\text{rf}})_{\text{minimum}} = \frac{B_0}{\sqrt{2}A_1}\exp\left(1+\frac{\lambda}{2C_2d}\right), \tag{4}$$

$$p_{\text{turning}} = \frac{1}{A_1 d\left(1-\frac{\lambda}{4C_2d}D\right)}\exp(2/D),$$

$$(U_{\text{rf}})_{\text{turning}} = \frac{B_0 D}{2\sqrt{2}A_1\left(1-\frac{\lambda}{4C_2d}D\right)}\exp(2/D),$$

$$\text{where } D = [\sqrt{1+(8dC_2/\lambda)}-1]. \tag{5}$$

In order to determine the position of the inflection point on the breakdown curve, the second derivate of Eq. (3) together with the condition $d^2U_{\text{rf}}/dp^2=0$ is used and the obtained expressions are given by

$$p_{\text{inflection}} = \frac{\left(1+\frac{\lambda}{4C_2d}\right)}{A_1 d}\exp\left(2+\frac{\lambda}{2C_2d}\right),$$

$$(U_{\text{rf}})_{\text{inflection}} = \frac{B_0}{2\sqrt{2}A_1}\exp\left(2+\frac{\lambda}{2C_2d}\right). \tag{6}$$

The above expressions can be applied to determine the scaling for the pressure and the breakdown voltage corresponding to the minimum, to the turning point, and to the inflection point on the breakdown curve. Standard description of the rf breakdown is given by Kihara's theory[15] and we shall use it here to compare to the results of our PIC simulations.

## III. PARTICLE-IN-CELL/MONTE CARLO SIMULATIONS

The simulation codes used in this work are the one-dimensional bounded electrostatic PIC codes with Monte Carlo treatment of collisional processes. PIC modeling techniques have been described in details in many publications (see, for example, Refs. 27–29), so only a brief description will be given here.

It is well known that for a rarefied gas or plasma, where correlations between particles are sufficiently weak, the time evolution of distribution functions is governed by the Boltzmann equation:

$$\frac{\partial f}{\partial t} + \nu\frac{\partial f}{\partial \mathbf{x}} - \frac{\mathbf{eE}}{m_e}\cdot\frac{\partial f}{\partial \nu} = \left(\frac{\partial f}{\partial t}\right)_{\text{coll}}. \tag{7}$$

Obtaining numerical solutions to the Boltzamnn equation under general conditions is a difficult computational problem. One widely used method to solve the Boltzmann equation for realistic gas discharges where electric field has to be calculated in a self-consistent manner is the PIC method.[29] In the PIC method, a group of electrons or ions is represented by a single simulation particle, the so-called superparticle. Each superparticle can represent $10^8$–$10^{12}$ real particles and the motion of each particle is assumed to follow Newton's law. The equations of motion for the superparticles are given by

$$\ddot{\mathbf{x}}_j = -\frac{q_j}{m_j}\boldsymbol{\nabla}\phi, \tag{8}$$

$$\varepsilon_0\nabla^2\phi = e\int d^3\nu f(\mathbf{x},\mathbf{v},t) - \rho_0, \tag{9}$$

where $\mathbf{x}_j=\mathbf{x}_j(t)$ is the position of the $j$th superparticle at the time $t$, $q_j$ and $m_j$ are its charge and mass, and $\rho_0$ is the charge density background due to oppositely charged species. The right-hand-side terms of Eq. (8) are therefore evaluated from the interpolation of $\phi$ values at neighboring grid points (force weighting), whereas the value of charge density in the right-hand side of Eq. (9) at each grid point is evaluated from the charges of neighboring particles (particle weighting). For these weighting processes to be accurate, a sufficient number of simulation particles must be present in each grid cell.

To simulate collisional plasmas using PIC method, the Monte Carlo collision method has been widely adopted.[27,30] As we use $10^6$ superparticles for each target species, computing the collision probability for all the particles at each time step can be computationally very expensive. Instead, a more efficient method designated as the null collision method is used in the codes.[27,29,30] For each type of projectile we can determine a total collision probability independent of particle energy and position as

$$P_t = 1-\exp(-\nu_{\max}dt), \tag{10}$$

where the maximum collision frequency is given by

$$\nu_{\max} = N_g\max_{\varepsilon}[\sigma_t(\varepsilon)\nu(\varepsilon)]. \tag{11}$$

In the above equation, $N_g$ is the spatially uniform neutral density, $\nu(\varepsilon)$ is the incident speed of a particle with energy $\varepsilon$, $dt$ is the time interval, and the total cross section $\sigma_t(\varepsilon)$ represents the sum over all processes $j$:

$$\sigma_t(\varepsilon) = \sum_j \sigma_j(\varepsilon). \tag{12}$$

The number of projectile particles $dn$ taking part in collisions at each time step is given by the total collision probability

$$dn = P_t n, \tag{13}$$

and these particles are chosen at random from the particle list. The type of collision for each particle is determined by a random number. Further details concerning differential cross sections for ionization and elastic scattering of electrons, fractional energy loss corresponding to the scattering events, transformations from the center of mass to the laboratory frame, and so on are described in Ref. 30.

We have simulated the operation of an argon CCP source with cylindrical electrodes. The inner electrode is capacitively coupled to rf power supply through a blocking capacitor. The upper electrode is grounded. Such a reactor is asym-

metric in the sense that the grounded electrode is larger than the powered one. All simulations have been carried out with argon as a filling gas. Neutral atoms were assumed to be uniformly distributed throughout the simulation domain with a Maxwellian velocity distribution at room temperature (0.026 eV). The gas pressure was varied from a few millitorr to a few Torr, while the electrode gaps belonged to the centimeter domain. Depending on the gas pressure, the time step $dt$ was of the order of about $10^{-12}$ s. One million computer particles were used initially in each simulation.

In order to determine the breakdown voltage, we use the fact that the breakdown is not an instantaneous phenomenon. Breakdown occurs over a finite period of time which is determined by the balance between creation of charged species by ionization and their loss via collisional processes and diffusion to the walls. For each value of the gas pressure, the time servitude of the electron density was observed, and depending on its increasing or decreasing nature, the interval in which the breakdown voltage lies could be found through trial and error process. Thus, for each value of the gas pressure several simulations were performed.

Choices of boundary conditions depend on the physical conditions of the boundary walls and electrodes. When an electron reaches the boundary, it is assumed to be absorbed. For an ion, it is also assumed to be adsorbed, but secondary electrons may be emitted with a probability $\gamma_i$ depending on the impinging ion energy. It was recently shown that the secondary emission characteristics of the electrodes have little effects on the right-hand side of the Paschen curve or the position of the curve minimum, but strongly affect the slope of the left-hand side of the breakdown curve.[20,24,25] Having in mind that the secondary emission processes are very important in determining the breakdown,[20,22] in our simulations both electron impact and ion induced secondary emission processes at the surface are included.

### A. Electron impact secondary emission

In our simulations we use a Vaughan-based secondary electron production[31,32] that includes energy and angular dependence as well as a full emission spectrum including reflected and scattered primaries. This is a more accurate model of secondary electron production. The electron impact secondary emission may be represented by the secondary emission coefficient that is equal to the flux of the emitted electrons normalized to the initial flux. It is given by

$$\delta(\varepsilon,\theta) = \delta_{\max 0}\left(1 + \frac{k_{s\delta}\theta^2}{2\pi}\right)(we^{1-w})^k, \tag{14}$$

where $w$ is the normalized energy expressed as

$$w = \frac{\varepsilon - \varepsilon_0}{\varepsilon_{\max 0}(1 + k_{sw}\theta^2/2\pi) - \varepsilon_0}, \tag{15}$$

where $\varepsilon$ is the incident energy of a particle and $\theta$ is its angle of incidence measured perpendicular to the surface, $\delta_{\max}$ is the peak secondary emission coefficient corresponding to the energy $\varepsilon_{\max}$ and normal incidence. The exponent $k$ is derived from a curve-fit analysis, $\varepsilon_0$ is the secondary emission threshold, $k_{s\delta}$ and $k_{sw}$ are the surface-smoothness parameters

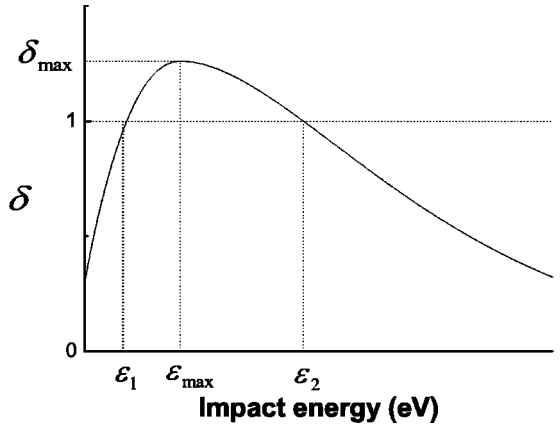


FIG. 2. The secondary emission coefficient $\delta$, defined as the ratio of ejected to incident electrons, as a function of the impact energy of electrons at normal incident to the surface. In our calculations the peak value of the secondary emission coefficient is $\delta_{\max}=1.2$ and the corresponding maximum energy $\varepsilon_{\max}=400$ eV.

(both can vary between 0 for rough surfaces and 2 for polished surfaces). Typical values are close to 1. In our simulations, $k=0.62$ for $w<1$ and $k=0.25$ for $w\geqslant 1$, the peak normal secondary emission in copper is $\delta_{\max 0}=1.2$ with $\varepsilon_{\max 0}=400$ eV and $\varepsilon_0=15$ eV. Figure 2 shows a schematic graph of the secondary emission coefficient. Having gained energy from the electric field, the electrons strike the surface with an impact energy $\varepsilon$ and when this energy lies between energies $\varepsilon_1$ and $\varepsilon_2$ (see Fig. 2), the first and second crossover energy, respectively, of the secondary electron yield curve, the secondary emission coefficient $\delta$ will be greater than unity. In this case a net gain of secondary electrons occurs.[33–35]

### B. Ion induced secondary emission

It is well known that at low pressure and small electrode separations, the loss rate of electrons to the walls is large, so surface effects such as electron impact and ion induced secondary emission processes are very important in determining breakdown. The secondary electron emission from a surface under the action of an ion is described by the coefficient quantifying the number of secondary electrons produced at the cathode per ion usually known as the electron yield per ion and denoted by $\gamma_i$. Although, this coefficient depends on the cathode material and the gas[22,34,36] it was often assumed that $\gamma_i$ is constant.[19,20,37,38]

In order to correct this deficiency, we implement both the energy and the angular dependence of the coefficient $\gamma_i$. The energy dependence of the coefficient $\gamma_i$ is based on the expression that was suggested by Phelps and Petrović[36] and later modified by Phelps *et al.*[39] (see Fig. 3):

$$\gamma_i(\varepsilon_i) = \frac{0.006\varepsilon_i}{1 + (\varepsilon_i/10)} + 1.05\times 10^{-4}\frac{(\varepsilon_i - 80)^{1.2}}{1 + (\varepsilon_i/8000)^{1.5}}, \tag{16}$$

where $\varepsilon_i$ is the incident energy of the ion. It is clear from Fig. 3 that there is a difference between the solid curve that shows fits to the experimental beam data and the dashed curve that represents the assumed $\gamma_i$ value of 0.08 for argon.

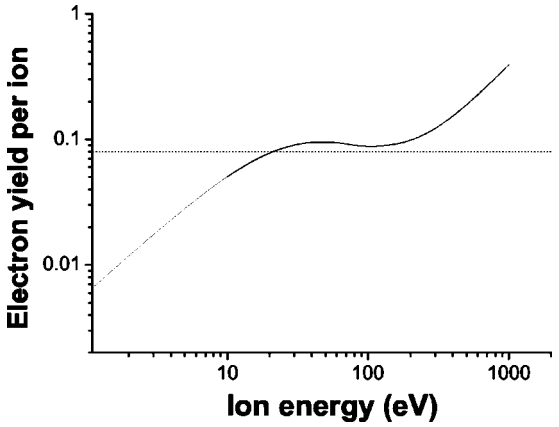


FIG. 3. The electron yield per $Ar^+$ incident on various dirty metal surfaces vs particle energy. Solid line is obtained by using energy dependence of the yield per ion expressed by Eq. (16) (taken from Ref. 36) and dashed line corresponds to an assumed average of 0.08 for argon.

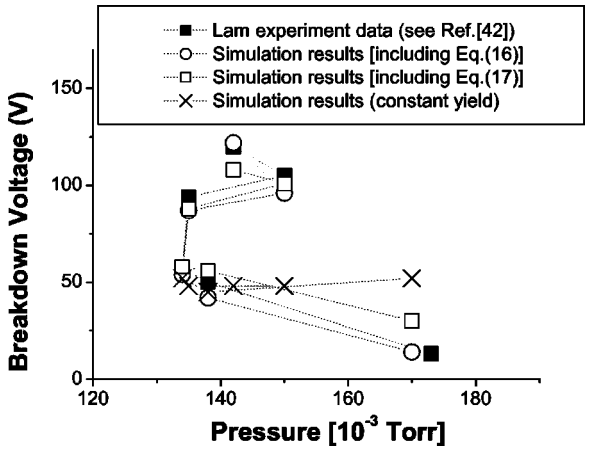


FIG. 4. The breakdown voltage vs the gas pressure for argon rf discharges at 27 MHz and the electrode separation of 1.6 cm. The experimental data (Ref. 42) are presented by solid symbols and compared with our simulation results obtained by using XPDC1 code including energy and/or angular dependent model for the yield per ion and presented by open symbols. Simulation results obtained by using constant value of the yield per ion are given by crosses.

The energy dependent yield per ion is attributed to an Auger process called kinetic ejection.[36]

According to the angular dependence of the coefficient suggested by Thieberger *et al.*,[40] Thomas[41] and Radmilović *et al.*[33,34] we assume that the angular dependence of the electron yield per ion $\gamma_i$ is described by

$$\gamma_i(\varepsilon_i, \theta) = \gamma_i(\varepsilon_i)\cos^{-1}\theta, \tag{17}$$

where $\theta$ is its angle of incidence measured with respect to the surface normal.

## IV. RESULTS AND DISCUSSIONS

### A. Pressure effect

As we have already emphasized, there is a range for which there is a multivalued dependence of the breakdown voltage on the gas pressure in the low-pressure region to the left-hand side of the breakdown curve's minimum. In our calculations we were primarily concerned with the conditions to the left of the breakdown Paschen minimum where secondary emission processes dominate.

For the rf breakdown to occur it is necessary either to apply a sufficiently large rf voltage that would induce secondary electron emission from electrodes or to enhance the pressure, i.e., to supply a large number of gas molecules in the path of exiting electrons. Therefore, at a voltage larger than the voltage that corresponds to the turning point, the breakdown curve moves to the region of larger pressure, i.e., ambiguity region arises. In Kihara's theory,[15] the sudden increase of the breakdown curve is attributed to the losses due to diffusion. In our simulations, the differences in the voltage versus the pressure dependence are due to different contribution of electron production at the surface of the cathode which may be partially associated with improved secondary yield model which is not a part of the analytical theory. However, the prediction of the sudden increase of the breakdown voltage is due to the same basic reasons as in Kihara's theory.

Figure 4 shows a characteristic breakdown curve of argon rf discharges at 27 MHz and the electrode separation of 1.6 cm. Our simulation results were obtained by using XPDC1 code and taking into account only energy dependence of the coefficient $\gamma_i$ [see Eq. (16)] (open circles) and simulation results obtained by using again XPDC1 code including both energy and angular dependence of the coefficient $\gamma_i$ [see Eq. (17)] (open squares) and compared with Lam experiment data[42] (solid symbols). As can be observed from Fig. 4, in both cases there is a good agreement between experimental and simulation results, while simulation results attained involving both energy and angular dependence of the coefficient $\gamma_i$ [given by Eq. (17)] better correspond to the experimental data.

We also present results obtained by using XPDC1 code for a constant value of the yield per ion ($\gamma_i = 0.2$) (crosses). Obviously, simulation results obtained by not taking into account energy and/or angular dependence of the electron yield per ion are in serious disagreement with the experimental data. These results indicate that, in simulations, changing of the slope of the left-hand branch of the breakdown curve can be treated only if energy and/or angular dependence of the yield per ion are included.

Expression (5) can be used to estimate the position and the breakdown voltage associated with the turning point on the breakdown curve. From the measurements we get that the turning point occurs at a pressure of 150 mTorr with the breakdown voltage of 105 V, which is in very good agreement with values of 150 mTorr and 96 V for the pressure and the breakdown voltage, respectively, obtained from simulation results. These values show a good agreement with the breakdown voltage of 94 V obtained by putting modified molecular constants taken from Ref. 18 into Eq. (5), but differ from the very high breakdown voltage of 161 V acquired by using molecular constants presented in Ref. 15. Explanation for such a discrepancy lies in the fact that at low gas pressure electron emission from electrodes plays a very important role in the breakdown and that the model described in Ref. 15 has not included this effect. Another rea-

son that causes discrepancy is the fact that Kihara[15] assumed the electron diffusion to be isotropic. In Refs. 19 and 25 it was shown that the breakdown data will be affected by the fact that the diffusion of electrons in gases is anisotropic as found originally by Parker and Lowke[43] and independently by Skullerud.[44] However, for high frequency breakdown the relevant phenomena will be those found for electron diffusion in rf fields (see, for example, Refs. 45 and 46).

In Fig. 5 we show comparisons between the experimental data[24] (solid symbols) and our simulation results (open symbols) for the breakdown voltage as a function of the gas pressure for argon rf discharges at 13.56 MHz for three different gap spacings. Calculations were carried out by using XPDC1 code involving both energy and angular dependence of the yield per ion [see Eq. (17)]. For all the three values of the electrode separation, a good agreement between the experimental[24] and the simulation results is achieved especially in the part to the left of the breakdown curve's minimum where the secondary emission processes are crucial in determining breakdown. For the region of the right-hand branch of the breakdown curve, one can assume that the secondary electron emission processes do not participate in the rf gas breakdown and we may call this part of the breakdown curve an emission-free branch. Therefore, distinctions between the experimental and the simulation results that can be noticed to the right of the breakdown minimum are not due to our secondary emission model.

At the electrode separation of 1.4 cm, values of the breakdown voltage corresponding to the turning point of 148 V (from the experimental results) and 138 V (from the simulation results), for the same pressure of 0.26 Torr, are in disagreement with the very high voltage of 348 V obtained by using molecular constants from Ref. 15 and very low voltage of 76 V attained applying revised molecular constants presented in Ref. 18. Similarly, for the minimum of the breakdown curve, the experimental results provide a value of 61 V while simulation results give the value of 66 V and both differ from the very high breakdown voltage of around 339 V obtained by using molecular constants from Ref. 15 and from a very low value of 44 V when molecular constants from Ref. 18 were used. Disagreements between our simulation results and the results obtained by using theoretical expressions (4)–(6) with molecular constants taken from Ref. 15 or Ref. 18, indicate that values of molecular constants have to be modified.

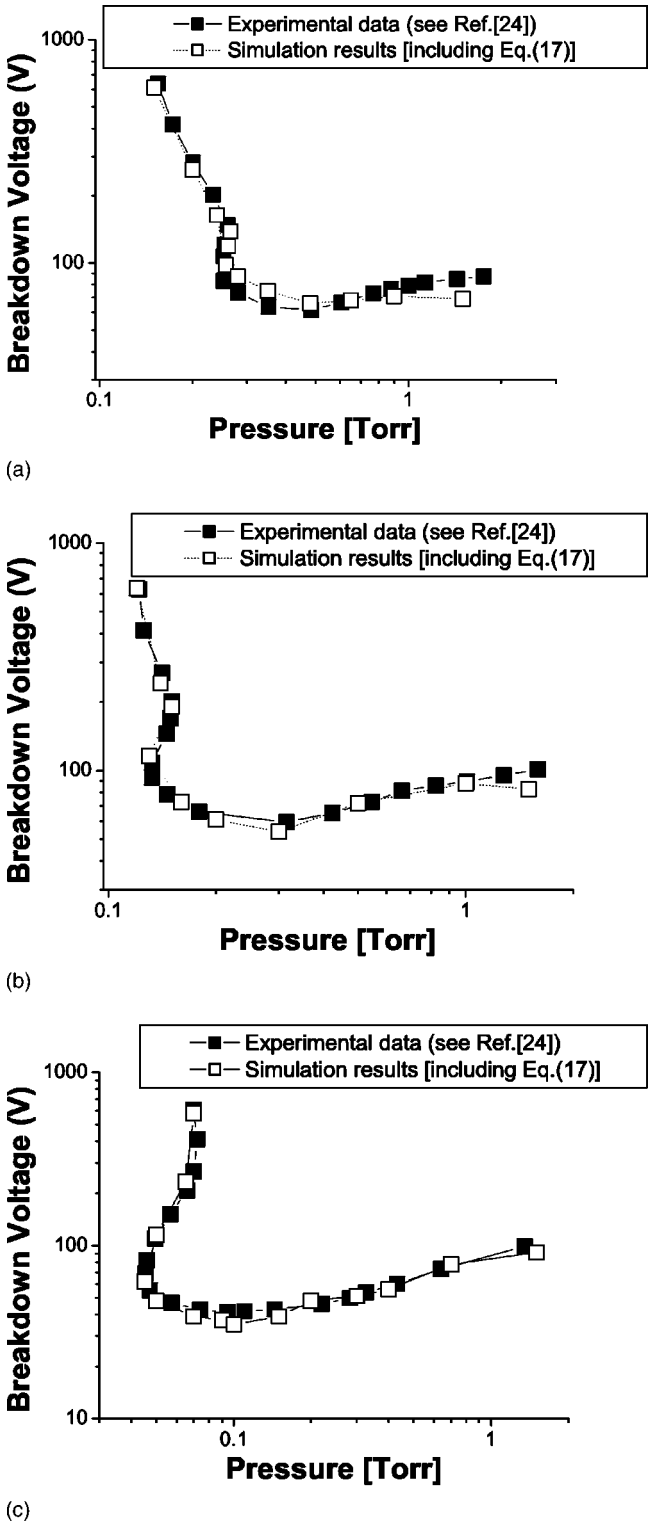


FIG. 5. Breakdown voltge as a function of the gas pressure for the electrode gap size of (a) 1.4 cm, (b) 2 cm, and (c) 2.9 cm. Results of our calculations performed using XPDC1 code including energy and angular dependence of the yield per ion [see Eq. (17)] are given by open symbols and compared with the experimental data presented in Ref. 24.

### B. Frequency effect

In order to investigate the dependence of the breakdown voltage on the frequency, calculations were performed keeping the rf current constant and varying the frequency from 13.56 to 54.4 MHz at the gas pressure of 250 mTorr. The operation of the discharge described in Ref. 47 was in a low current mode and modeling of that discharge should follow the same laws as for the breakdown conditions, since breakdown is the low current limit of the discharge in this regime. We have made simulations for the exact conditions of the experiments and have observed adequacy of the same model as used for the breakdown itself. Simulation results (open symbols) and their comparison with the experimental data[47] (solid symbols) are presented in Fig. 6. Similar trends are observed in simulation and experimental results while simulation results are systematically lower than the experimental data. Although the same gap size is used in both the cases,

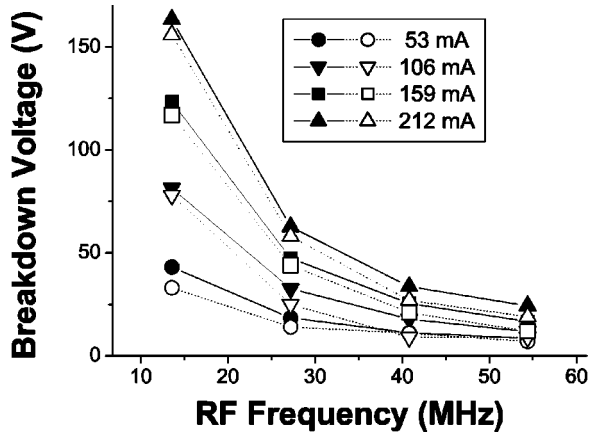


FIG. 6. Breakdown voltage plotted against rf frequency. Calculations were performed at the gas pressure of 250 mTorr and the electrode separation of 2 cm for four different values of the rf current. Simulation results are shown by open symbols while experimental results (Ref. 47) are given by solid symbols.

the temperature and the electrode materials used in the experiments are unknown.[47] Differences in temperature and secondary emission coefficients are believed to cause the breakdown voltage difference between simulations and experimental results observed in Fig. 6.

As expected, the breakdown voltage decreases with an increasing frequency and both experimental and simulation results indicate that the breakdown voltage is a strong function of the frequency for all the current levels. The experimental data shown in Fig. 6 for the three highest current values provide $U_{\mathrm{rf}} \propto f^{-1.4}$ dependence, while for the lowest current value give $U_{\mathrm{rf}} \propto f^{-1.2}$ dependence. For the three highest current values simulation results give the same frequency dependence of the breakdown voltage as obtained from the measurements and a slightly weaker dependence described by $U_{\mathrm{rf}} \propto f^{-1.1}$ for the rf current of 0.53 mA. Results of a fluid model simulation from Ref. 47 provide a $U_{\mathrm{rf}} \propto f^{-1.2}$ dependence for the high current value and a weaker dependence for the low current values and are not shown in Fig. 6.

## V. CONCLUSION

In this paper, we were especially interested in the influence of the secondary emission properties of the electrodes on the breakdown voltage in rf discharges during breakdown. Since it is not straightforward to vary the secondary emission coefficient in experiments, XPDC1 code with improved secondary emission model was utilized to study these effects. Our simulation results clearly show the effect of the secondary emission processes on the breakdown voltage and confirm that there is a low-pressure region where a multivalued dependence of the breakdown voltage on the gas pressure exists. We have shown that the multivalued nature of the left-hand branch of the breakdown curve can be achieved by only taking into account the energy dependence of the coefficient that describes ion induced secondary emission production both, with or without angular dependence of the yield per ion. Results obtained including both energy and angular dependence of the yield per ion show better agreement with the experimental data. Our simulation results also reveal that the secondary emission characteristic of the electrodes has very little effect on the right-hand branch of the breakdown curve or the position of the curve minimum, but strongly affects the slope of the left-hand branch of the breakdown curve. Values of the breakdown voltages corresponding to the turning point and the minimum on the breakdown curves obtained from experimental and simulation results are very obtained by using theoretically derived expressions allow us to conclude that a more accurate determination of molecular constants is needed.

In studying the effect of frequency variation in high-frequency low-pressure argon discharges we have obtained satisfactory agreement between our simulation results and experimental data. As a result of their analysis, a frequency scaling law at constant current is proposed.

## ACKNOWLEDGMENTS

This work was supported by the Lam Research Corporation and Tera-level Nano Devices Project, 21c Frontier R&D Program of Korea Ministry of Science and Technology. The authors are grateful for very useful discussions with Dr. Branislav Radjenović. One of the authors (M.R.R.) is grateful to Dr. Zoran Petrović for reading the manuscript and giving useful comments, and to project MNTRS (Project No. 1478) which led to collection and testing of some of the data on secondary electron yields required for the present simulation.

[1] J. R. Ligenza, J. Appl. Phys. **36**, 2703 (1965).
[2] A. C. Eckbreth and J. W. Davis, Appl. Phys. Lett. **21**, 25 (1972).
[3] C. O. Brown and J. W. Davis, Appl. Phys. Lett. **21**, 480 (1972).
[4] M. J. Druyvesteyn and F. M. Penning, Rev. Mod. Phys. **12**, 87 (1940).
[5] Yu. P. Raizer, *Gas Discharge Physics* (Springer, Berlin, 1991).
[6] V. A. Godyak and R. B. Piejak, Phys. Rev. Lett. **65**, 996 (1990).
[7] W. M. Moreu, *Semiconductor Litography: Principles, Practices and Materials* (Plenum, New York, 1988).
[8] D. L. Flamm, V. M. Donnelly, and D. E. Ibbotson, J. Vac. Sci. Technol. B **1**, 23 (1983).
[9] Y. Catherine and P. Couderc, Thin Solid Films **144**, 265 (1986).
[10] R. S. Yalamanchi and G. K. M. Thutupalli, Thin Solid Films **164**, 103 (1988).
[11] Yu. P. Raizer, M. N. Schneider, and N. A. Yatsenko, *Radio-Frequency Capacitive Discharges* (CRC, New York, 1995).
[12] H. B. Smith, C. Charles, and R. W. Boswell, J. Appl. Phys. **82**, 561 (1997).
[13] K. Kitajima, Y. Takeo, Z. Lj. Petrović, and T. Makabe, Appl. Phys. Lett. **77**, 489 (2000).
[14] H. C. Kim and J. K. Lee, Phys. Rev. Lett. **93**, 085003 (2004).
[15] T. Kihara, Rev. Mod. Phys. **24**, 45 (1952).
[16] S. Githens, Phys. Rev. **57**, 822 (1940).
[17] S. N. Sen and A. K. Ghosh, Indian J. Phys. **36**, 605 (1962).
[18] V. A. Lisovskiy and V. D. Yegorenkov, J. Phys. D **27**, 2340 (1994).
[19] M. Sato and M. Shoji, Jpn. J. Appl. Phys., Part 1 **36**, 5729 (1997).
[20] H. B. Smith, C. Charles, and R. W. Boswell, Phys. Plasmas **10**, 875 (2003).
[21] M. M. Turner, Phys. Rev. Lett. **75**, 1312 (1995).
[22] M. Ramilović-Radjenović, J. K. Lee, F. Iza, and G. Y. Park, J. Phys. D **38**, 950 (2005).
[23] F. Honh, W. Jacob, R. Beckmann, and R. Wilhelm, Phys. Plasmas **4**, 940 (1997).
[24] N. Yu. Kropotov, Yu. A. Kachanov, A. G. Reuka, V. A. Lisovskiy, V. D. Erorenkov, and V. Farenik, Sov. Tech. Phys. Lett. **14**, 159 (1988).
[25] V. A. Lisovskiy and V. D. Yegorenkov, J. Phys. D **31**, 3349 (1998).
[26] S. C. Brown and A. D. MacDonald, Phys. Rev. **76**, 1629 (1949).
[27] C. K. Bridsall, IEEE Trans. Plasma Sci. **19**, 65 (1991).

[28]V. Vahedi and M. Surendra, Comput. Phys. Commun. **87**, 179 (1995).
[29]J. P. Verboncoeur, M. V. Alves, V. Vahedi, and C. K. Birdsall, J. Comput. Phys. **104**, 321 (1993).
[30]S. Hamaguchi, IBM J. Res. Dev. **43**, 199 (1999).
[31]J. R. M. Vaughan, IEEE Trans. **36**, 1963 (1989).
[32]J. R. M. Vaughan, IEEE Trans. **40**, 830 (1993).
[33]M. Radmilović, V. Stojanović, and Z. Lj. Petrović, *The Book of Contributed Papers of the 20th Symposium of Physics of Ionized Gases, Zlatibor, September 2000*, edited by Z. Lj. Petrović, M. M. Kuraica, N. Bibić, and G. Malović (Public Enterprise of PTT "Serbia," Belgrade, 2002), Vol. I, p. 131.
[34]M. Radmilović-Radjenović, *The Physics of Ionized Gases: Invited Lectures, Topical Invited Lectures and Progress Reports of 21th Symposium of Physics of Ionized Gases, Soko Banja, August 2002*, edited by N. Bibić, T. Grozdanov, and M. Radović (Cigoja Printing Office, Belgrade, 2002), Vol. I, p. 107.
[35]A. Valfells, L. K. Ang, Y. Y. Lau, and R. M. Gilgenbach, Phys. Plasmas **7**, 750 (2000).
[36]A. V. Phelps and Z. Lj. Petrović, Plasma Sources Sci. Technol. **8**, R21 (1999).
[37]J. P. Boeuf, Phys. Rev. A **36**, 2782 (1987).
[38]F. Taccogna, S. Longo, and M. Capitteli, Phys. Plasmas **11**, 1220 (2004).
[39]A. V. Phelps, L. C. Pitchford, C. Pedoussat, and Z. Donko, Plasma Sources Sci. Technol. **8**, B1 (1999).
[40]P. Thieberger, A. L. Hanson, D. B. Steski, V. Zajic, S. Y. Zhang, and H. Ludewig, Phys. Rev. A **61**, 042901 (2000).
[41]E. W. Thomas, Nucl. Fusion **94**, 94 (1984) (special issue).
[42]J. W. Shon (private communication).
[43]J. H. Parker, Jr. and J. J. Lowke, Phys. Rev. **181**, 290 (1969).
[44]H. R. Skullerud, J. Phys. B **2**, 86 (1969).
[45]K. Maeda, T. Makabe, N. Nakano, S. Bzenić, and Z. Lj. Petrović, Phys. Rev. E **55**, 5901 (1997).
[46]Z. Lj. Petrović, Z. M. Raspopović, S. Dujko, and T. Makabe, Appl. Surf. Sci. **192**, 1 (2002).
[47]M. J. Colgant, M. Meyyappan, and D. E. Murnick, Plasma Sources Sci. Technol. **3**, 181 (1994).